Electrochemical Sensing Behavior of Graphdiyne Nanoflake Toward Uric Acid; A Quantum Chemical Approach

Misbah Asif
COMSATS Institute of Information Technology - Abbottabad Campus
Hasnain Sajid
University of Nottingham
Khurshid Ayub
COMSATS Institute of Information Technology - Abbottabad Campus
Mazhar Amjad Gilani
COMSATS Institute of Information Technology - MA Jinnah Campus: COMSATS University Islamabad - Lahore Campus
Mohammed Salim Akhter
University of Bahrain
Tariq Mahmood (mahmood@cuiatd.edu.pk)
COMSATS Institute of Information Technology - Abbottabad Campus https://orcid.org/0000-0001-8850-9992

Research Article

Keywords: Graphdiyne nanoflake, Uric acid, Biosensing, Density functional theory

Posted Date: June 2nd, 2021

DOI: https://doi.org/10.21203/rs.3.rs-542765/v1

Version of Record: A version of this preprint was published at Journal of Molecular Modeling on August 10th, 2021. See the published version at https://doi.org/10.1007/s00894-021-04860-8.

Electrochemical sensing behavior of graphdiyne nanoflake toward uric acid; a quantum chemical approach

Misbah Asif[1#], Hasnain Sajid[1#], Khurshid Ayub[1], Mazhar Amjad Gilani[2], Mohammed Salim Akhter[3] and Tariq Mahmood[1,3]*

[1]*Department of Chemistry, COMSATS University Islamabad, Abbottabad Campus, Abbottabad-22060, Pakistan*

[2]*Department of Chemistry, COMSATS University Islamabad, Lahore Campus, Lahore*

[3]*Department of Chemistry, College of Science, University of Bahrain, Bahrain*

*To whom correspondence can be addressed: E-mail: mahmood@cuiatd.edu.pk (T. M)

[#]Misbah Asif and Hasnain Sajid have equal contributions for first authorship

Abstract

Though, the gas sensing applications of graphdiyne have widely reported; however, the biosensing utility of graphdiyne needs to be explored. This study deals with the sensitivity of graphdiyne nanoflake (GDY) towards the uric acid (UA) within the density functional framework. The uric acid is allowed to interact with graphdiyne nanoflake from all the possible orientations. Based on these interacting geometries, the complexes are differentiated with naming *i.e*., UA1@GDY, UA2@GDY, UA3@GDY and UA4@GDY (Figure 1). The essence of interface interactions of UA on GDY is derived by computing geometric, energetic, electronic and optical properties. The adsorbing affinity of complexes is evaluated at ωB97XD/6-31+G(d,p) level of theory. The stabilities of the complexes are quantified through the interaction energies (E_{int}) with reasonable accuracy. The calculated E_{int} of the UA1@GDY, UA2@GDY, UA3@GDY and UA4@GDY complexes are -31.13, -25.87, -20.59 and -16.54 kcal/mol, respectively. In comparison with geometries, it is revealed that the higher stability of complexes is facilitated by π-π stacking. Other energetic analyses including symmetry adopted perturbation theory (SAPT0), noncovalent interaction index (NCI) and quantum theory of atoms in molecule (QTAIM) provided the evidence of dominating dispersion energy in stabilizing the resultant complexes. The HOMO-LUMO energies, NBO charge transfer and UV-vis analysis justify the higher electronic transition in UA1@GDY, plays a role of higher sensitivity of GDY towards the π-stacked geometries over all other possible interaction orientations. The present findings bestow the higher sensitivity of GDY towards uric acid via π-stacking interactions.

Keywords**:** Graphdiyne nanoflake; Uric acid; Biosensing; Density functional theory

Introduction

Uric acid (UA), a white crystalline substance was firstly discovered by Scheele et al, from kidney stone in 1776 [1]. Chemically, it is insoluble in water but converted to urate salts in acidic medium [2]. The living organisms release uricase enzyme which oxidizes the uric acid to generates carbon dioxide (CO_2) and hydrogen peroxide (H_2O_2) as a product [3]. Human does not possess uricase enzyme, thus the uric acid cannot be oxidized in human metabolism. The optimum level of uric acid in human body is kept stable naturally by the secretion. With the time and modification in the living standards, the consumption of purines has been increased seriously resulting the notable risk of hyperuricemia. The optimum level of uric acid in an adult human range from 1.5-7.0 mg/dL [4]. However, the deficiency or surplus of uric acid in the body causes increase in urate ions, the condition known as hyperuricemia which in turns responsible for cardiovascular and renal diseases, multiple sclerosis, optic neuritis, Alzheimer's disease, Parkinson's disease, hypertension, type II diabetes, tumor lysis syndrome and gout [5]. Therefore, the detection of uric acid in blood and urine can be a powerful indicator for early prevention of diseases. Hence, it is necessary to develop inexpensive, accurate and reliable sensors.

Literature reveals that the various sensors materials has been designed for the effective detection and removal of uric acid [6–8]. Stozhko et al*.,* [9] designed gold nanostructure-based sensor for the accurate detection of uric acid in blood. Rana et al*.,* [10] designed love wave acoustic device based on zinc oxide thin film for detection of uric acid in blood. Jain *et al.* synthesized the electrochemical sensor based on butylamine capped CZTS for nanoparticles the detection of UA [11]. Moreover, two-dimensional carbon sheets [12], metallic sensors [13] and nanocomposite [14] materials has been synthesized as effective sensors for the detection of uric acid.

Recently, it has been concluded that carbon-based materials including nanosheets and nanotubes are best suited for bio-sensing applications [15]. The high surface to volume ratio features the carbon materials a highly durable for the detection of biomolecules. Moreover, the selectivity of such systems is attained by the high charge carrier mobility of such materials [16]. Among all the carbon nanosheets, graphdiyne have fascinating electronic and structural properties. This non-natural stable carbon allotrope was first predicted in the year 1997 by Haley et al., [17]. In 2010, it was first synthesized by cross coupling reaction on the surface of copper. Graphdiyne exhibits remarkable geometric and electronic properties including chemical stability, high charge carrier mobility, good electrical conductivity and high chemical activity [18]. Owing to these properties, graphdiyne has been used widely in vast applications in the field of nanoelectronics, transistors, photocatalysis and gas sensors.

Graphdiyne nanoflake (GDY), smallest representative of graphdiyne sheet, has been used for sensing of variety of molecules including both experimental [19,20] and theoretical [21–23]. According to the literature survey, we couldn't find any report, either theoretical or experimental, to explain the sensing behavior or sensitivity of GDY towards uric acid molecule. Here, we intend to investigate the sensitivity of GDY for uric acid molecule at different conformations. The sensitivity of GDY for uric acid is quantified theoretically via geometric, energetic, electronic and optical properties.

Computational methodology

Gaussian09 [24] and GaussView5.0 [25] software's are used for the calculations and visualization of results, respectively. In order to locate the preferred interaction site, all the possible interaction orientations are studied. Among them, the geometries with least interaction are subjected to detail analysis. All the geometries are optimized at ωB97XD/6-31+G(d,p) level of theory. ωB97XD is a long range separated functional which is reported as a best method for accurate analysis of noncovalent interactions [26]. The interaction energies are calculated by using equation 1.

$$E_{int} = E_{UA@GDY} - (E_{GDY} + E_{UA}) \text{ -------} 1$$

Where, the E_{GDY}, E_{UA}, $E_{UA@GDY}$ are the representation for the energies of GDY, UA analyte and their complexes, respectively. Literature reveals that the calculation of interaction energy from equation 1 is many folds less than the desire accuracy [27]. Recently, the symmetry adopted perturbation theory (SAPT0) analysis is considered to be one of the best approaches to investigate the noncovalent interactions with higher accuracy [28]. In SAPT0 analysis, the noncovalent interaction energy splits into four meaningful components including induction (ind), electrostatic (elest), dispersion (dis) and exchange (exch) [29]. Psi4 [30] software is used to perform SAPT0 analysis. In order to visualize the noncovalent components physically between GDY and UA, a visualization approach; interaction index (NCI) [31] analysis is applied by using Multiwfn3.6 [32] software.

The effect of doping UA upon the electronic behavior of GDY is measured by analyzing the HOMO-LUMO orbitals and NBO charge transfer analysis prior and after complexation. According to literature, HOMO-LUMO gap varies on interaction with analytes due to the generation of new energy states between the existing orbitals that can be justified via density of state (DOS) analysis. Therefore, DOS analysis has been performed using GaussSum software. Lastly, the variation in the optical properties of GDY after adsorbing UA is measured by time dependent density functional theory (TD-DFT) calculations.

Results and discussions

Geometric and thermodynamic analysis

All possible orientations of UA and GDY nanoflake have been tested to obtain the thermodynamically stable complexes *i. e.*, UA1@GDY, UA2@GDY, UA3@GDY and UA4@GDY. The stable geometries of UA@GDY complexes are shown in Figure 1. According to literature, the interacting distance (D_{int}) and interaction energies (E_{int}) play a significant role in describing interaction behavior. These interaction parameters of complexes are listed in Table 1. The UA1@GDY complex is mainly stabilized via stacking π-π interactions and N-H···π interactions. Owing to these dual interactions, the interaction energy of UA1@GDY complex is significantly higher than that of side orientations. The interaction energy of UA1@GDY complex is -31.13 kcal/mol. On the other hand, the N-H···π interactions or weak hydrogen bonding (C-H···O) take part in stabilizing the UA2@GDY, UA3@GDY and UA4@GDY complexes. Due to the absence of π-stacking, the interaction energies of UA2@GDY, UA3@GDY and UA4@GDY complexes reduce to -25.87, -20.59 and -16.54 kcal/mol, respectively. The interaction energies of UA2@GDY, UA3@GDY and UA4@GDY complexes gradually decrease with the decrease in the number of N-H···π interactions, respectively. For example, there are two N-H···π interactions in UA2@GDY complex, while this number reduce to one and zero in UA3@GDY and UA4@GDY complexes, respectively (refer to Figure 1). After interaction energies, the interaction distance is another important parameter to demonstrate the interaction strength. According to the literature, the interaction strength is inversely related to the interaction distances between adsorbent and adsorbate [7]. The multiple interactions are possible in UA@GDY complexes, but the discussion is limited to the least interaction distances of all the complexes for the ease of understanding. Although, the strongest interaction is noticed in UA1@GDY complex, however, the interaction distance is surprisingly high which might be due to the domination of π-stacking. The interaction distance in UA1@GDY complex is 2.78 Å. However, the interaction distance of UA and GDY in UA2@GDY complex is 2.15 Å which is gradually increase with decreasing interaction energies in UA3@GDY and UA4@GDY complexes where the interaction distances are 2.20 and 2.60 Å, respectively. From the results, it can clearly be noticed that the dispersion energy plays a significantly role in stabilizing the complexes which is quite higher in UA1@GDY complex. The contribution of dispersion in stabilizing complexes is discussed in the subsequent SAPT0 section.

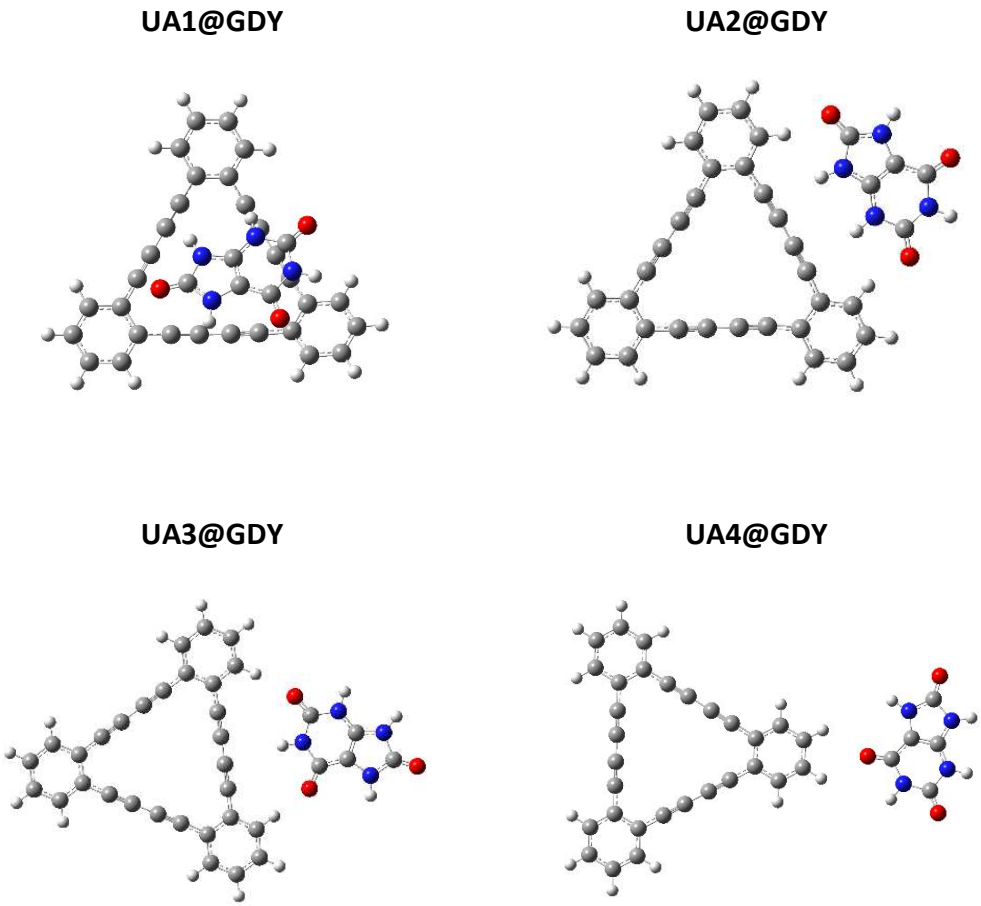

Fig. 1. Optimized geometries (with interaction distances in Å) of UA@GDY complexes.

Table 1. The results of most stable optimized UA@GDY complexes.

Properties	GDY	UA1@GDY	UA2@GDY	UA3@GDY	UA4@GDY
A_{int}	---	H_{49}-C_{34}	O_{58}-H_8	O_{55}-H_8	O_{55}-H_{10}
D_{int} (Å)	---	2.78	2.15	2.20	2.60
E_{int} (kcal/mol)	---	-31.13	-25.87	-20.59	-16.54
SAPT0 analysis (kcal/mol)					
E_{est}	---	-11.48	-15.05	-7.52	-2.31
E_{exch}	---	18.28	17.00	7.34	2.03
E_{ind}	---	-4.40	-6.60	-2.21	-0.65
E_{dis}	---	-24.59	-10.45	-6.13	-2.36
E_{SAPT0}	---	-22.19	-15.12	-8.53	-3.29
HOMO-LUMO energies (eV)					
HOMO	-7.71	-7.67	-7.84	-7.59	-7.56
LUMO	-0.68	-0.96	-0.93	-0.57	-0.58
E_g	7.03	6.71	6.90	7.02	6.97
NBO charge transfer (e^-)					
NBO	---	0.822	-0.78	-0.697	-0.10
UV-Vis analysis					
λ_{exct} (eV)	3.96	3.91	3.93	3.96	3.95
λ_{max} (nm)	312	317	315	312	313
f	0.99	0.63	1.01	1.05	1.12

Symmetry adopted perturbation theory (SAPT0) analysis

SAPT0 analysis elaborates the noncovalent interactions by splitting into four meaningful components i.e., electrostatic (E_{est}), exchange (E_{exch}), induction (E_{ind}) and dispersion (E_{dis}) [33]. However, the total SAPT0 refers the sum of all the four noncovalent components (see eq. 2).

$$E_{SAPT} = (-E_{est}) + (E_{exch}) + (-E_{ind}) + (-E_{dis}) \text{----- 2}$$

Here, the exothermic nature of electrostatic, induction and dispersion components attribute the attraction between UA and GDY which stabilizes the complexes. However, exchange is endothermic, which reflects the repulsive forces and destabilizing nature of the complexes [34]. The results of SAPT0 (Table1 or Figure 2) illustrate that the dispersion component dominates in UA1@GDY complexe which is -24.59 kcal/mol. However, the contribution of dispersion in UA2@GDY, UA3@GDY and UA4@GDY complexes is -10.45, -6.13 and -2.36 kcal/mol, respectively which is appreciably low as compared to UA1@GDY complex. Like dispersion, electrostatic component also plays significant contribution for the stability of complexes. The contribution of E_{est} component in UA1@GDY, UA2@GDY, UA3@GDY and UA4@GDY is -11.48, -15.05, -7.52 and -2.31 kcal/mol, respectively. The highest E_{est} in UA2@GDY is probably due to the multiple N-H···π

or weak hydrogen bond (C-H···O) interactions (vide supra). The total E_{SAPT0} of UA1@GDY, UA2@GDY, UA3@GDY and UA4@GDY are -22.19, -15.12, -8.53 and -3.29 kcal/mol, respectively. Finally, the trend of total SAPT0 is well accord with the sequence of interaction energies that is; UA1@GDY> UA2@GDY> UA3@GDY> UA4@GDY.

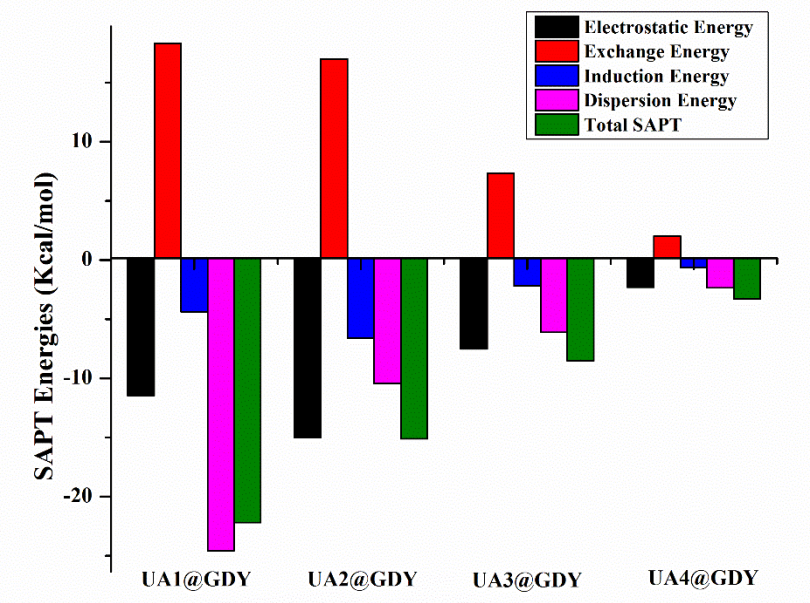

Fig. 2. Graphical representation of the contribution of SAPT0 components in UA@GDY complexes.

Non-covalent interaction index analysis (NCI)

NCI is a visual approach, performed to visualize the attractive and repulsive forces between adsorbate (UA) and adsorbent (GDY) [35]. The NCI results mainly consist of 3D isosurfaces and 2D RDG graph, as shown in Figure 3. In NCI results, the strength of interaction is distinguished with red, green and blue colors which represent the weak dispersion forces, strong hydrogen bonding and steric repulsive forces, respectively. From the NCI isosurfaces (Figure 3), it can be noticed that deep green flaky surfaces appear between stacked UA and GDY, attributing the domination of dispersion forces in UA1@GDY complex. Moreover, the bunch of green spikes between -0.01 and 0.01 au of RDG graph of UA1@GDY complex also indicates the existence of dispersion component. However, these green spikes reduce in other side interactions of UA and GDY which attributes the lowering of dispersion contribution. In case of UA3@GDY complex, the blue patches between oxygen of UA and hydrogen of GDY in 2D isosurface and blue peak at -0.02 au of RDG graph indicate the presence of hydrogen bonding. Results shows red peak at 0.02 au of all RDG 2D graphs indicates the presence of exchange/repulsive forces in the complexes,

however, these repulsive forces are intramolecular rather than intermolecular. These NCI results are well accord with the energetic and SAPT0 results.

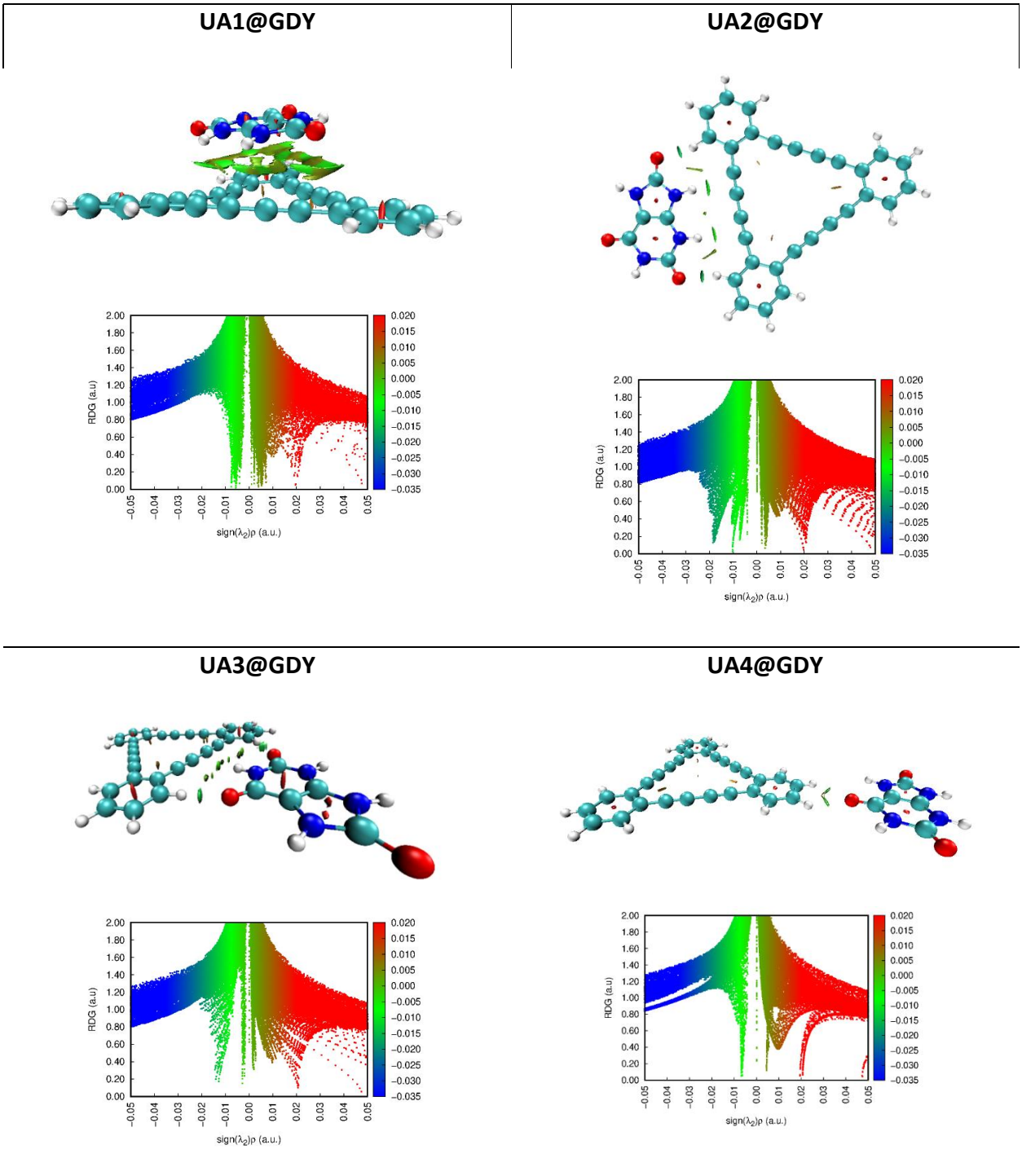

Fig. 3. NCI iso-surfaces (isovalue = 0.5 au) and RDG spectra of UA@GDY complexes.

Table 2. QTAIM parameters of UA@GDY complexes (unit of values is au).

No.	A_{ad}	ρ	$\nabla^2\rho$	G	V	H
UA1@GDY						
72	N53-C39	0.005	0.016	0.003	-0.003	0.0005
74	O58-C40	0.006	0.020	0.004	-0.003	0.0007
98	O58-C38	0.006	0.021	0.004	-0.003	0.0008
107	N52-C3	0.005	0.015	0.003	-0.003	0.0004
121	H50-C30	0.006	0.020	0.004	-0.003	0.0011
122	H54-C33	0.007	0.022	0.005	-0.004	0.0006
128	H49-C34	0.007	0.025	0.005	-0.003	0.0014
UA2@GDY						
68	O56-H16	0.018	0.050	0.0130	-0.0134	-0.00039
82	H49-C41	0.007	0.019	0.0040	-0.0030	0.00010
105‘	H50-C33	0.010	0.028	0.0059	-0.0049	0.0010
121	O58-H8	0.018	0.051	0.0132	-0.0137	-0.00045
UA3@GDY						
72	H48-C33	0.014	0.046	0.011	-0.010	0.0004
93	O55-H8	0.002	0.010	0.002	-0.001	0.0007
118	O56-H16	0.012	0.044	0.010	-0.009	0.0007
UA4@GDY						
86	O55-H10	0.007	0.026	0.006	-0.004	0.0010
99	O55-H7	0.006	0.025	0.005	-0.004	0.0011

Quantum theory of atoms in molecule

The nature and strength of interactions between interacting moieties can be differentiated via QTAIM analysis [35]. In QTAIM results (Table 2 & Figure 4), the electronic density (ρ), Laplacian electron density ($\nabla^2\rho$), and the sum of electron densities (H) are important parameters to differentiate between the covalent and noncovalent interactions. H can be calculated by the equation below:

$H=V+G$

The values of ρ, $\nabla^2\rho$ & H are listed in Table 2 while their critical points (CP) are shown in Figure 4. Our QTAIM results are well consistent with SAPT0 and NCI analysis which reveal that the weak noncovalent (dispersion) interaction dominates in the complexes because the value of electronic density (ρ) is smaller than 0.1 au along with the small positive values of Laplacian ($\nabla^2\rho$) for all critical points. The average values of ρ in UA1@GDY, UA2@GDY, UA3@GDY and UA4@GDY

complexes are 0.006, 0.018, 0.013 and 0.065 au, respectively. The values of H are positive in UA@GDY complexes, indicate the presence of weak noncovalent interactions. However, the value of H is negative for the critical point 68 and 121 of UA2@GDY complexes which attributes the strong noncovalent (hydrogen bonding) interaction between the oxygen of UA and hydrogen of GDY.

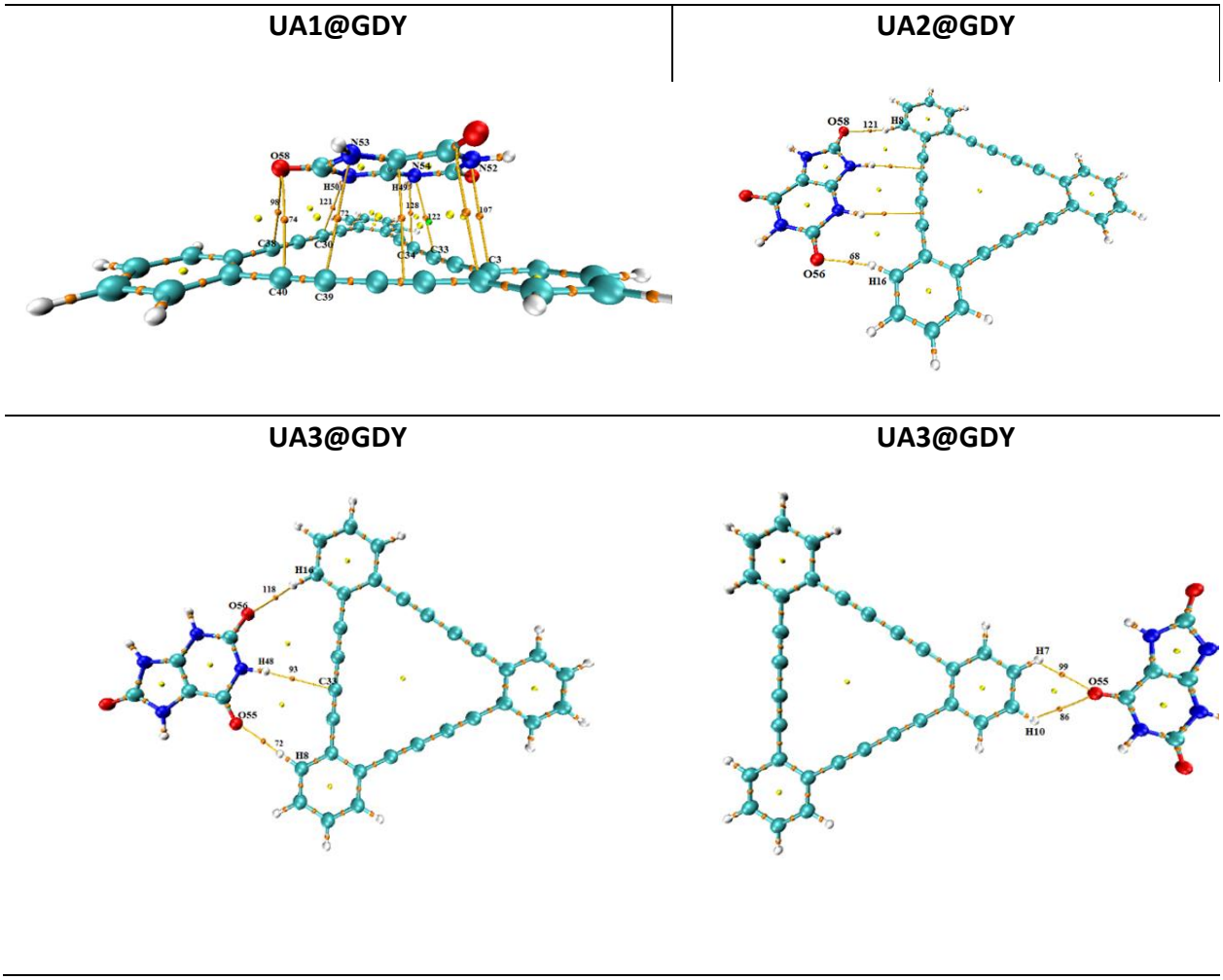

Fig. 4. QTAIM analysis of UA@GDY complexes.

Electronic Properties

The HOMO and LUMO energies of isolated and complexed GDY are simulated in order to measure the variation in electronic behavior upon complexation. The energies of HOMO and LUMO orbitals along with their differences or energy gaps (E_g) are listed in Table 1. The HOMO and LUMO energies of isolated GDY are -7.71 and -0.68 eV, respectively while its E_g is 7.03 eV, well consistent with the earlier reports [36,37]. The HOMO and LUMO gap of GDY is appreciably changed upon complexation with uric acid. The observed Eg of UA1@GDY, UA2@GDY, UA3@GDY

and UA4@GDY complexes are 6.71, 6.90, 7.02 and 6.97 eV, respectively. The variation in the HOMO-LUMO gap of GDY indicates the change in conductivity on interaction with uric acid. Expectedly, the more pronounced change is observed in E_g of UA1@GDY complex which might be due to the involvement of HOMO orbital of stacked uric acid molecule (see Figure 5). Moreover, the new HOMO orbitals are generated closer to the Fermi level upon complexation. One can infer from the DOS spectra (Figure 5), the new HOMO orbitals are generated at –7.67, -7.84, -7.59 and -7.56 eV in UA1@GDY, UA2@GDY, UA3@GDY and UA4@GDY complexes, respectively. These new energy states cause the lowering of H-L gaps of complexes, attribute the increase in conductivity. The surge in conductivity reflects the provoke in charge transfer between interacting moieties. Therefore, the NBO charge transfer has been calculated for deeper analysis of electron density shifting between GDY and uric acid molecule. The charge transfer between GDY and UA is calculated by natural bond orbital charge transfer (NBO) [38] calculations and the results are given in Table 1. The negative sign with NBO charges illustrates that the charges transfer from GDY to uric acid and opposite is true for positive charges. Expectedly, the largest amount of charge transfer (0.82 e^-) is noticed in UA1@GDY complex which is due to the least H-L gap. In UA2@GDY, UA3@GDY and UA4@GDY complexes, the appreciable amount of charges transfers from GDY towards the electronegative oxygen atom of UA. The amount of charges transferred UA2@GDY, UA3@GDY and UA4@GDY complexes are -0.78, -0.697 and -0.10 e^-, respectively. Similar to the geometric and energetic analysis, the electronic properties indicate that the adsorption of uric acid molecule on the GDY is facilitated by π-π stacking.

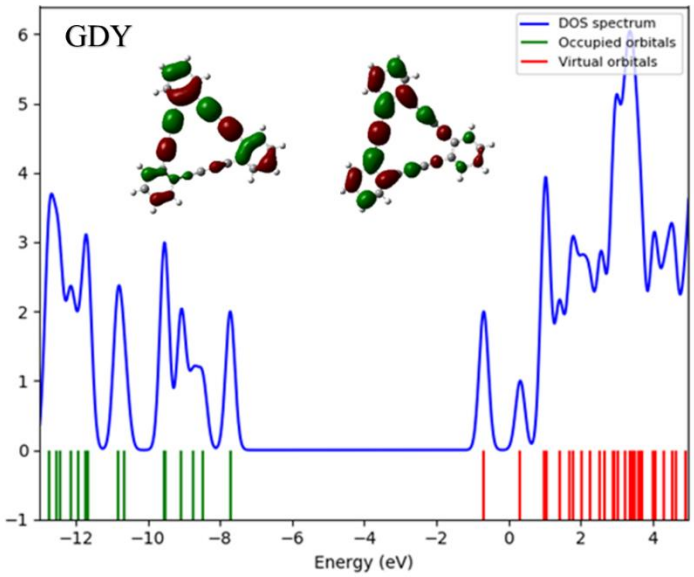

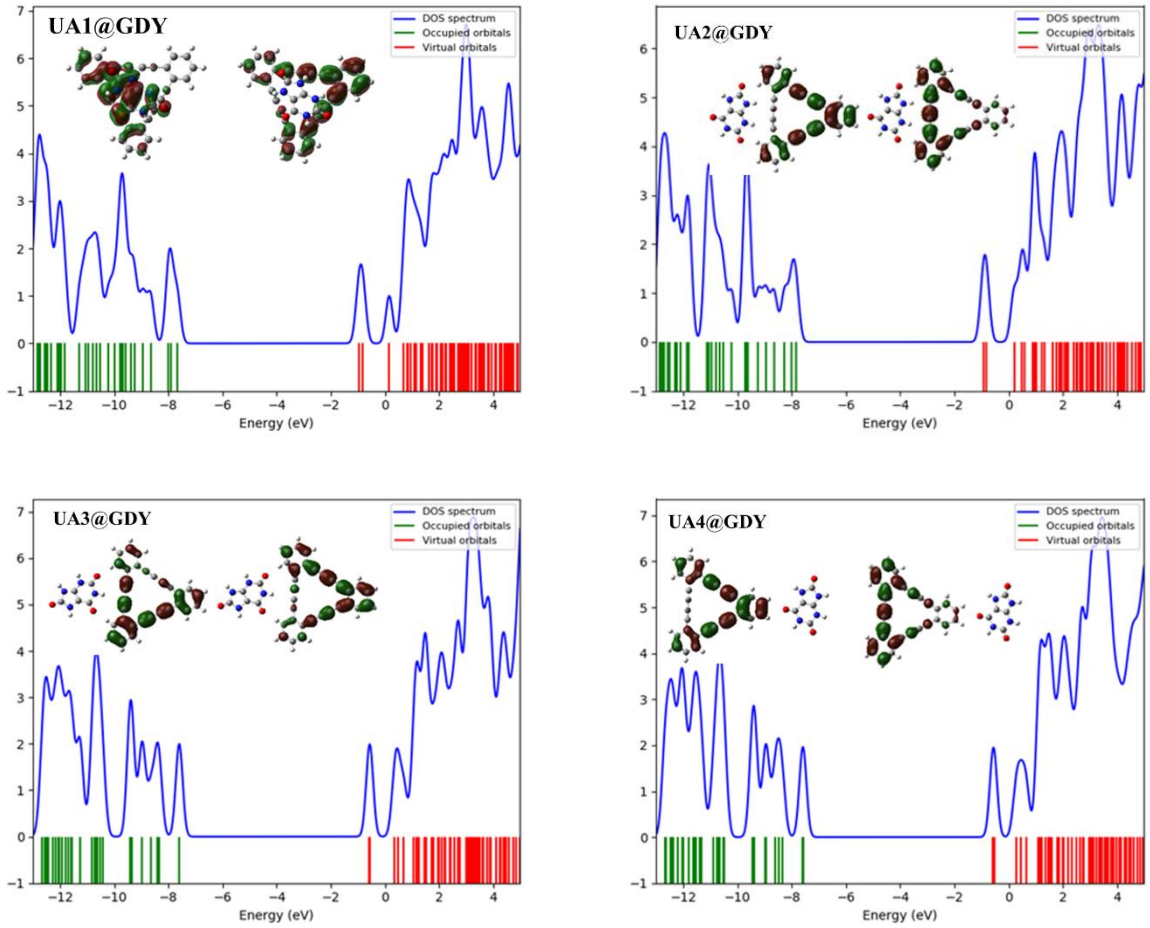

Fig. 5. DOS spectra with HOMO LUMO isosurfaces of UA@GDY complexes.

UV-vis absorption spectra

In adsorption studies, the UV-vis absorption analysis plays a crucial role because variation in absorption wavelength is expected because of the overlapping of the wave-functions of interacting species [39]. Time dependent density functional theory (TD-DFT) at ωB97XD/6-31+G(d, p) level of theory has been used for calculating the maximum absorbance (λ_{max}) of GDY prior a and after complexation. UV-vis results including maximum absorbance (λ_{max}), excitation energy (λ_{exct}) and oscillator strength (*f*) are listed in Table 1. The UV-vis spectra of bare and complexed GDY is displayed in Figure 6. The UV-Vis results reveal that the maximum absorbance of bare GDY takes place at 312 nm along with the transition energy of 3.96 eV, good accord with the literature [27]. The values of λ_{max} are red shifted to 317, 315 and 313 nm in UA1@GDY, UA2@GDY, and UA4@GDY complexes, respectively. The red shift of λ_{max} attributes the easy transition of π-electrons upon complexation which is revealed by the lowering of excitation energies. The λ_{exct} of UA1@GDY, UA2@GDY, and UA4@GDY complexes are 3.91, 3.93 and 3.95

eV, respectively. However, the λ_{max} is not significantly changed in UA3@GDY which is well consistent with the least variation in H-L gap of particular complex. Besides, the oscillator strength is expected to be deviate largely with increasing interaction strength [39]. The largest deviation of oscillator strength, difference between *f* of GDY and UA1@GDY complex is 0.36, indicates the strongest interaction and agrees well with the energetic and electronic properties.

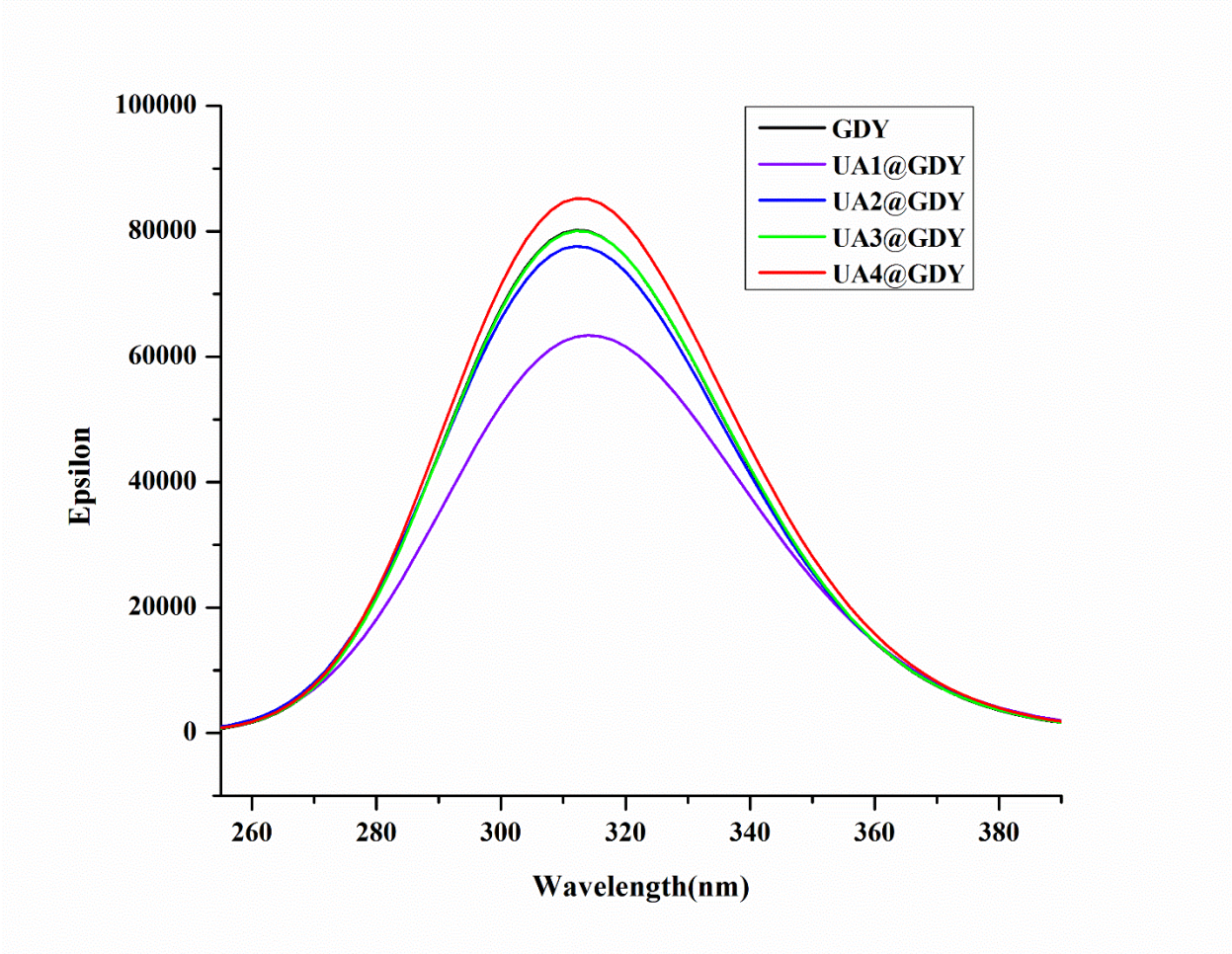

Fig. 6. UV-vis spectra of UA@GDY complexes.

4 Conclusions

This report demonstrates the sensitivity of graphdiyne nanoflake (GDY) towards a biomolecule (Uric acid) using density functional theory; ωB97XD/6-31+G(d, p) level of theory. Here, the uric acid molecule interacts with GDY from four different orientations and the complexes are named as; UA1@GDY, UA2@GDY, UA3@GDY and UA4@GDY. The sensitivity of GDY towards uric acid from all possible positions is quantify via energy calculations of all geometries and the variations

in electronic behavior. The calculated E_{int} of the UA1@GDY, UA2@GDY, UA3@GDY and UA4@GDY complexes are -31.13, -25.87, -20.59 and -16.54 kcal/mol, respectively. The higher stability of UA1@GDY complex comes through the higher dispersion involvement by π-stacked interactions. The SAPT0 analysis also indicates that the higher contribution of dispersion component in UA1@GDY complex. The contribution of dispersion component in UA1@GDY, UA2@GDY, UA3@GDY and UA4@GDY complexes are -24.59, -10.45, -6.13 and -2.36 kcal/mol, respectively. Similarly, the presence of dispersion energy is evident by the NCI and QTAIM analysis. The largest variation in HOMO-LUMO energy gap, highest NBO charge transfer and largest red shifted λ_{max} in UA1@GDY complex attributes the higher affinity of GDY via π-stacking rather than side interactions.

Acknowledgements

Authors acknowledge the Higher Education Commission of Pakistan and COMSATS University, Abbottabad Campus for financial support of this work.

Supplementary material

Supplementary data associated with this article can be found, in the online version, at http://dx.doi.org/

Author Declarations

Funding: Funding for this project was provided by Higher Education Commission of Pakistan.

Conflicts of interest/Competing interests: Authors declare no competing interests

Ethics approval: NA

Consent to participate: NA

Consent for publication: All authors agree for the publication of the manuscript

Availability of data and material: All relevant data are given in the supporting information file.

Code availability: Software used are commercially available

Authors' contributions: **Misbah Asif and Hasnain Sajid** (Acquisition and analysis of data; manuscript drafting). **Mazhar Amjad Gilani and Mohammed Salim Akhter** (Acquisition and analysis of data) **Khurshid Ayub** (Study conception and design; Critical revision), **Tariq Mahmood** (Supervision; Study conception and design; Critical revision)

References

[1] C.R. MacKenzie, Gout and Hyperuricemia: an Historical Perspective, Curr. Treat. Options Rheumatol. 1 (2015) 119–130.

[2] W.R. Wilcox, A. Khalaf, A. Weinberger, I. Kippen, J.R. Klinenberg, Solubility of uric acid and monosodium urate, Med. Biol. Eng. 10 (1972) 522–531.

[3] J. Galbán, Direct determination of uric acid in serum by a fluorometric-enzymatic method based on uricase, Talanta. 54 (2001) 847–854.

[4] M. Arvand, M. Hassannezhad, Magnetic core–shell Fe3O4@SiO2/MWCNT nanocomposite modified carbon paste electrode for amplified electrochemical sensing of uric acid, Mater. Sci. Eng. C. 36 (2014) 160–167.

[5] J.S. Cameron, F. Moro, H.A. Simmonds, Gout, uric acid and purine metabolism in paediatric nephrology, Pediatr. Nephrol. 7 (1993) 105–118.

[6] D. Lakshmi, M.J. Whitcombe, F. Davis, P.S. Sharma, B.B. Prasad, Electrochemical Detection of Uric Acid in Mixed and Clinical Samples: A Review, Electroanalysis. 23 (2011) 305–320.

[7] H. Sajid, T. Mahmood, K. Ayub, High sensitivity of polypyrrole sensor for uric acid over urea, acetamide and sulfonamide: A density functional theory study, Synth. Met. 235 (2018) 49–60.

[8] S. Qi, B. Zhao, H. Tang, X. Jiang, Determination of ascorbic acid, dopamine, and uric acid by a novel electrochemical sensor based on pristine graphene, Electrochim. Acta. 161 (2015) 395–402.

[9] N. Stozhko, M. Bukharinova, L. Galperin, K. Brainina, A Nanostructured Sensor Based on Gold Nanoparticles and Nafion for Determination of Uric Acid, Biosensors. 8 (2018) 21.

[10] L. Rana, R. Gupta, M. Tomar, V. Gupta, Highly sensitive Love wave acoustic biosensor for uric acid, Sensors Actuators B Chem. 261 (2018) 169–177.

[11] S. Jain, S. Verma, S.P. Singh, S.N. Sharma, An electrochemical biosensor based on novel butylamine capped CZTS nanoparticles immobilized by uricase for uric acid detection, Biosens. Bioelectron. 127 (2019) 135–141.

[12] C. Zhao, Y. Jiao, F. Hu, Y. Yang, Green synthesis of carbon dots from pork and application as nanosensors for uric acid detection, Spectrochim. Acta Part A Mol. Biomol. Spectrosc. 190 (2018) 360–367.

[13] S. Qu, Z. Li, Q. Jia, Detection of Purine Metabolite Uric Acid with Picolinic-Acid-Functionalized Metal–Organic Frameworks, ACS Appl. Mater. Interfaces. 11 (2019) 34196–

34202.

[14] C.-L. Sun, H.-H. Lee, J.-M. Yang, C.-C. Wu, The simultaneous electrochemical detection of ascorbic acid, dopamine, and uric acid using graphene/size-selected Pt nanocomposites, Biosens. Bioelectron. 26 (2011) 3450–3455.

[15] Z. Zhu, L. Garcia-Gancedo, A.J. Flewitt, H. Xie, F. Moussy, W.I. Milne, A Critical Review of Glucose Biosensors Based on Carbon Nanomaterials: Carbon Nanotubes and Graphene, Sensors. 12 (2012) 5996–6022.

[16] J. Peña-Bahamonde, H.N. Nguyen, S.K. Fanourakis, D.F. Rodrigues, Recent advances in graphene-based biosensor technology with applications in life sciences, J. Nanobiotechnology. 16 (2018) 75.

[17] M.M. Haley, S.C. Brand, J.J. Pak, Carbon Networks Based on Dehydrobenzoannulenes: Synthesis of Graphdiyne Substructures, Angew. Chemie Int. Ed. English. 36 (1997) 836–838.

[18] Q. Peng, J. Crean, L. Han, S. Liu, X. Wen, S. De, A. Dearden, New materials graphyne, graphdiyne, graphone, and graphane: review of properties, synthesis, and application in nanotechnology, Nanotechnol. Sci. Appl. (2014) 1.

[19] N. Parvin, Q. Jin, Y. Wei, R. Yu, B. Zheng, L. Huang, Y. Zhang, L. Wang, H. Zhang, M. Gao, H. Zhao, W. Hu, Y. Li, D. Wang, Few-Layer Graphdiyne Nanosheets Applied for Multiplexed Real-Time DNA Detection, Adv. Mater. 29 (2017) 1606755.

[20] J. Li, C. Wan, C. Wang, H. Zhang, X. Chen, 2D Material Chemistry: Graphdiyne-based Biochemical Sensing, Chem. Res. Chinese Univ. 36 (2020) 622–630.

[21] S. Khan, H. Sajid, K. Ayub, T. Mahmood, Sensing of toxic Lewisite (L 1 , L 2 , and L 3) molecules by graphdiyne nanoflake using density functional theory calculations and quantum theory of atoms in molecule analysis, J. Phys. Org. Chem. (2020).

[22] P. Xu, N. Na, A. Mohamadi, Investigation the application of pristine graphdiyne (GDY) and boron-doped graphdiyne (BGDY) as an electronic sensor for detection of anticancer drug, Comput. Theor. Chem. 1190 (2020) 112996.

[23] V. Nagarajan, R. Chandiramouli, Investigation of NH 3 adsorption behavior on graphdiyne nanosheet and nanotubes: A first-principles study, J. Mol. Liq. 249 (2018) 24–32.

[24] J.R. Frisch, M. J. T., G. W. Schlegel, H. B. Scuseria, G. E. Robb, M. A. Cheeseman, G.A. Scalmani, G. Barone, V. Mennucci, B. Petersson, Gaussian 09, Rev. D. 0.1, Gaussian, Inc. Wallingford, CT, 2013.

[25] J. Dennington, Roy; Keith, Todd; Millam, GaussView 5.0, Semichem Inc., Shawnee Mission KS, 2009. (2009).

[26] Y. Li, L. Xu, H. Liu, Y. Li, Graphdiyne and graphyne: from theoretical predictions to practical construction, Chem. Soc. Rev. 43 (2014) 2572.

[27] S. Khan, H. Sajid, K. Ayub, T. Mahmood, High sensitivity of graphdiyne nanoflake toward detection of phosgene, thiophosgene and phosogenoxime; a first-principles study, J. Mol. Graph. Model. (2020) 107658.

[28] H. Cybulski, J. Sadlej, Symmetry-Adapted Perturbation-Theory Interaction-Energy Decomposition for Hydrogen-Bonded and Stacking Structures, J. Chem. Theory Comput. 4 (2008) 892–897.

[29] K. Szalewicz, Symmetry-adapted perturbation theory of intermolecular forces, Wiley Interdiscip. Rev. Comput. Mol. Sci. 2 (2012) 254–272.

[30] J.M. Turney, A.C. Simmonett, R.M. Parrish, E.G. Hohenstein, F.A. Evangelista, J.T. Fermann, B.J. Mintz, L.A. Burns, J.J. Wilke, M.L. Abrams, N.J. Russ, M.L. Leininger, C.L. Janssen, E.T. Seidl, W.D. Allen, H.F. Schaefer, R.A. King, E.F. Valeev, C.D. Sherrill, T.D. Crawford, Psi4: an open-source ab initio electronic structure program, Wiley Interdiscip. Rev. Comput. Mol. Sci. 2 (2012) 556–565.

[31] N.S. Venkataramanan, A. Suvitha, Nature of bonding and cooperativity in linear DMSO clusters: A DFT, AIM and NCI analysis, J. Mol. Graph. Model. 81 (2018) 50–59.

[32] T. Lu, F. Chen, Multiwfn: A multifunctional wavefunction analyzer, J. Comput. Chem. 33 (2012) 580–592.

[33] H. Sajid, F. Ullah, K. Ayub, T. Mahmood, Cyclic versus straight chain oligofuran as sensor: A detailed DFT study, J. Mol. Graph. Model. 97 (2020).

[34] I.K. Petrushenko, N.I. Tikhonov, K.B. Petrushenko, Graphene-BN-organic nanoflake complexes: DFT, IGM and SAPT0 insights, Diam. Relat. Mater. 107 (2020) 107905.

[35] J. N. Ghogomu, N. K. Nkungli, DFT Studies and Topological Analyses of Electron Density on Acetophenone and Propiophenone Thiosemicarbazone Derivatives as Covalent Inhibitors of Falcipain- 2, a Major Plasmodium Falciparum Cysteine Protease, Phys. Chem. Res. 5 (2017) 795–817.

[36] S. Khan, H. Sajid, K. Ayub, T. Mahmood, Adsorption behaviour of chronic blistering agents on graphdiyne; excellent correlation among SAPT, reduced density gradient (RDG) and QTAIM analyses, J. Mol. Liq. 316 (2020) 113860.

[37] S. Khan, M. Yar, N. Kosar, K. Ayub, M. Arshad, M.N. Zahid, T. Mahmood, First-principles study for exploring the adsorption behavior of G-series nerve agents on graphdyine surface, Comput. Theor. Chem. 1191 (2020) 113043.

[38] A.J. Stone, Natural Bond Orbitals and the Nature of the Hydrogen Bond, J. Phys. Chem. A. 121 (2017) 1531–1534.

[39] H. Sajid, T. Mahmood, M.H.R. Mahmood, K. Ayub, Comparative investigation of sensor application of polypyrrole for gaseous analytes, J. Phys. Org. Chem. (2019) e3960.

Figures

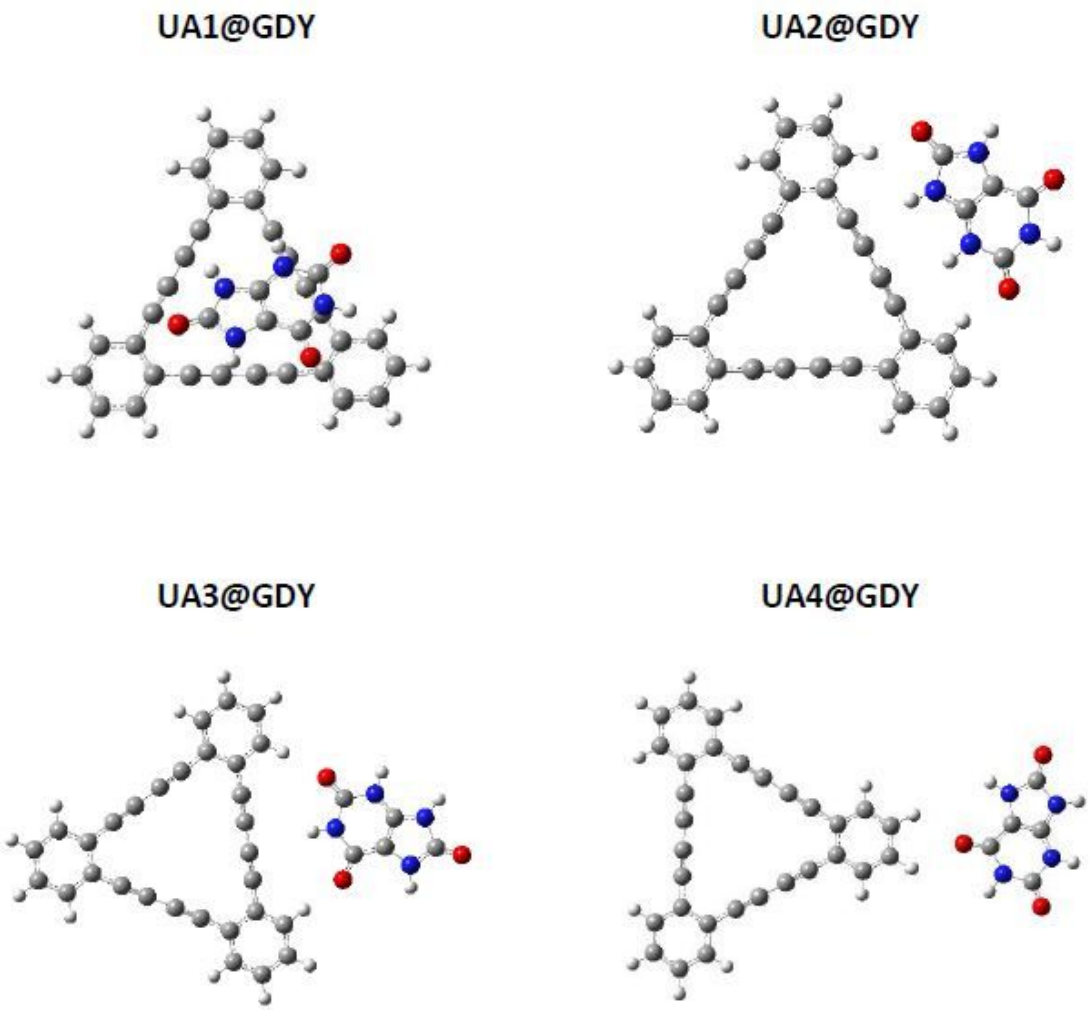

Figure 1

Optimized geometries (with interaction distances in Å) of UA@GDY complexes.

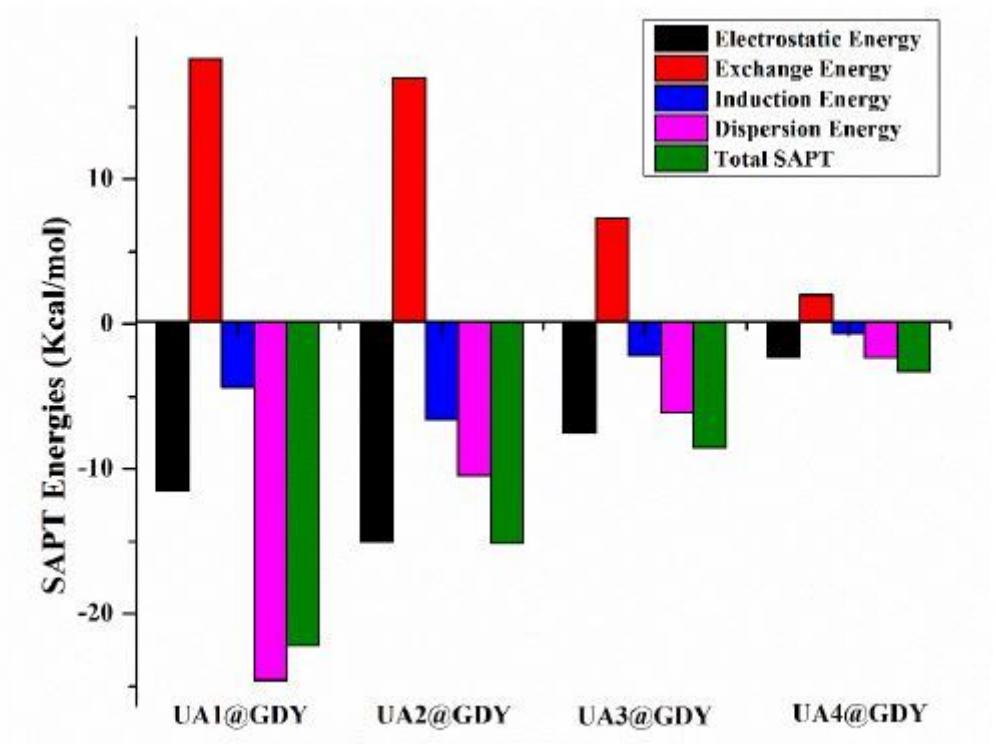

Figure 2

Graphical representation of the contribution of SAPT0 components in UA@GDY complexes.

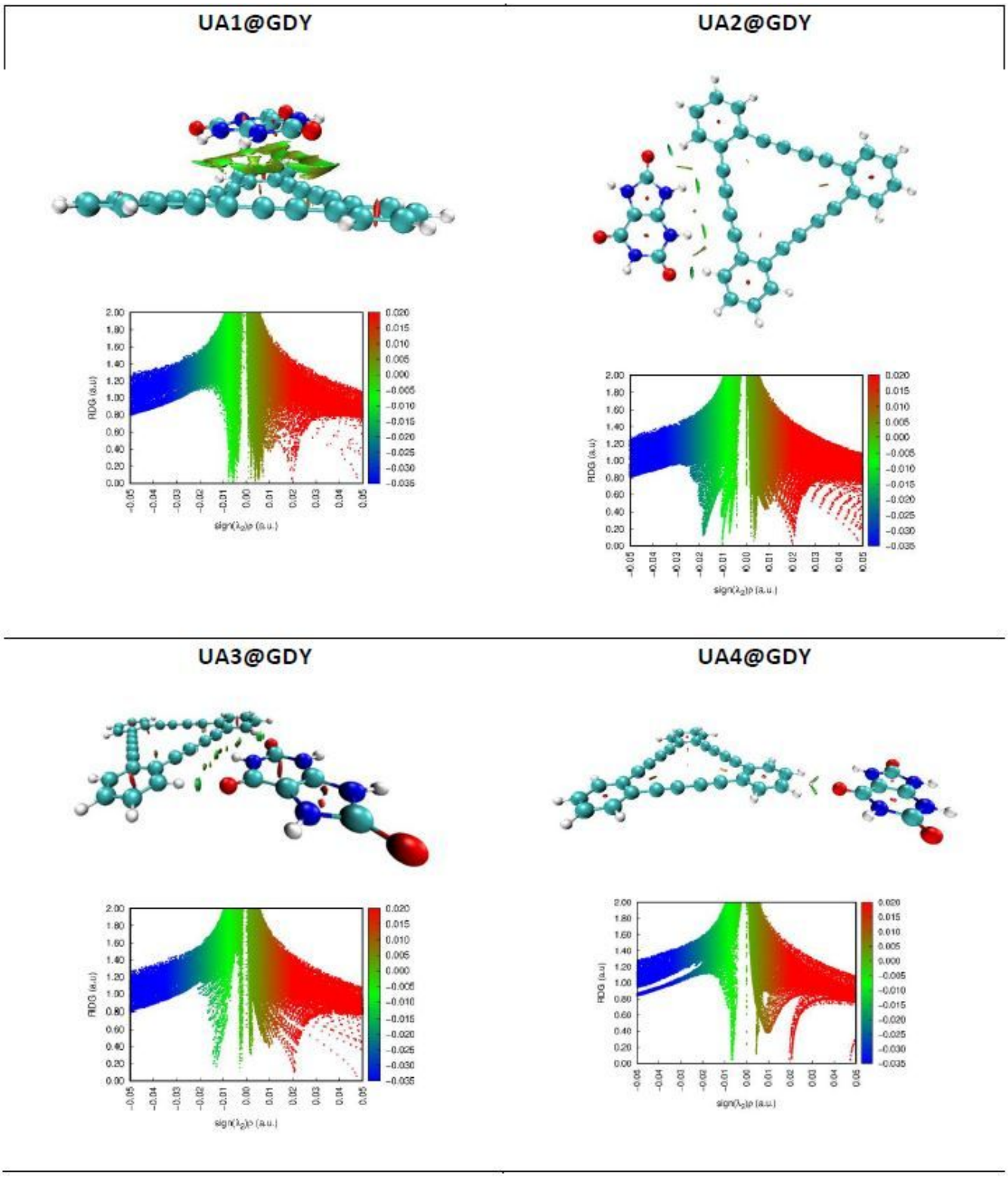

Figure 3

NCI iso-surfaces (isovalue = 0.5 au) and RDG spectra of UA@GDY complexes.

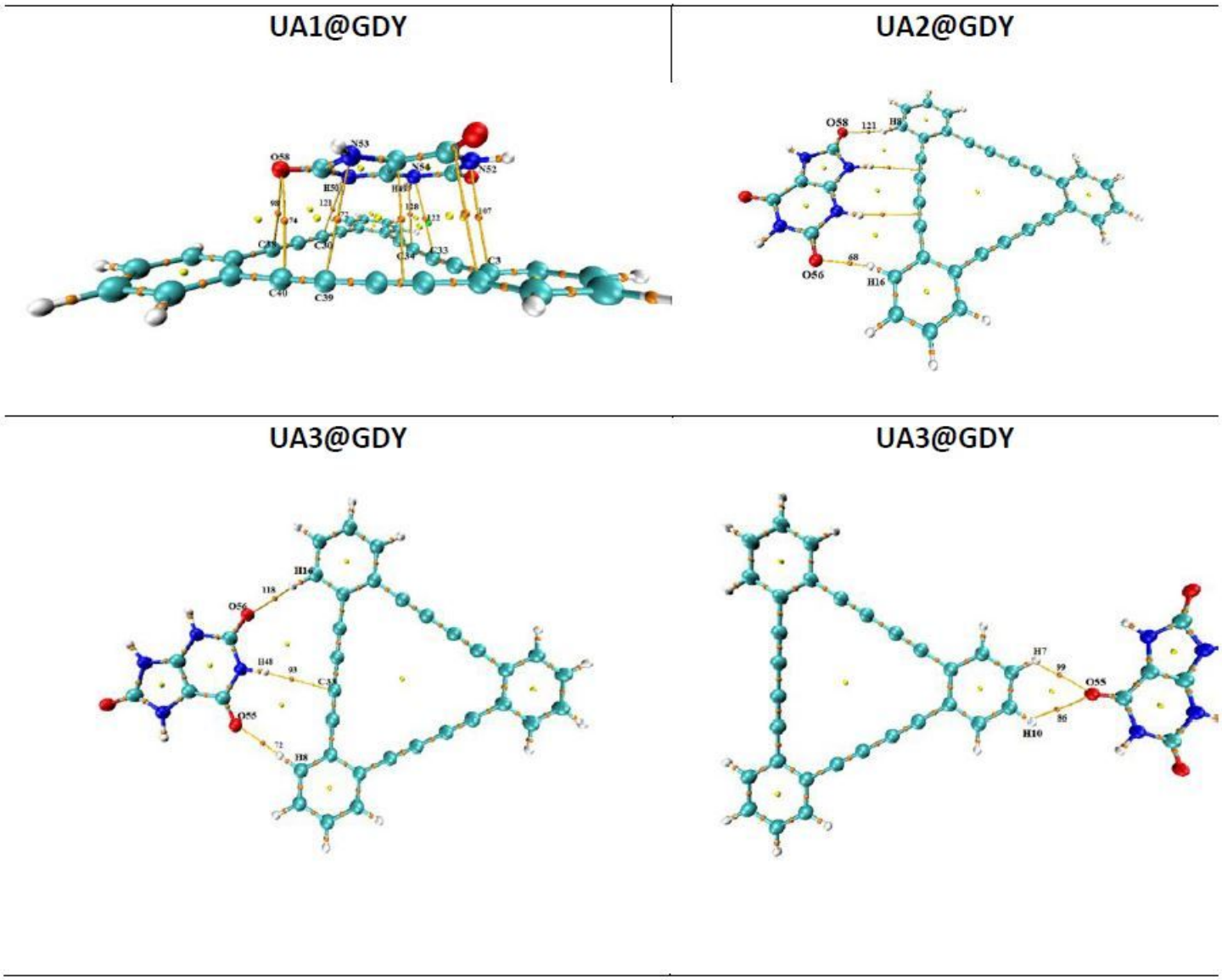

Figure 4

QTAIM analysis of UA@GDY complexes.

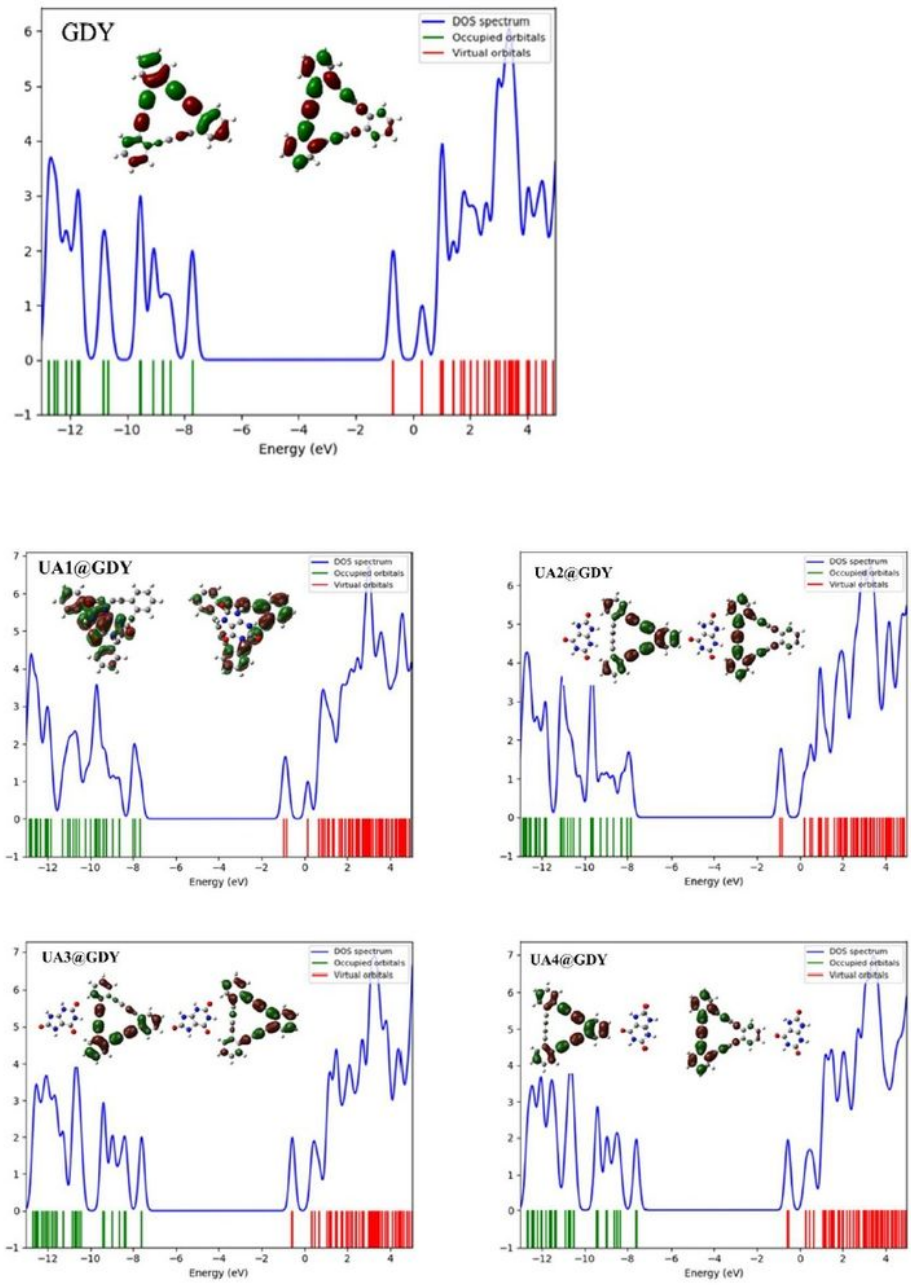

Figure 5

DOS spectra with HOMO LUMO isosurfaces of UA@GDY complexes.

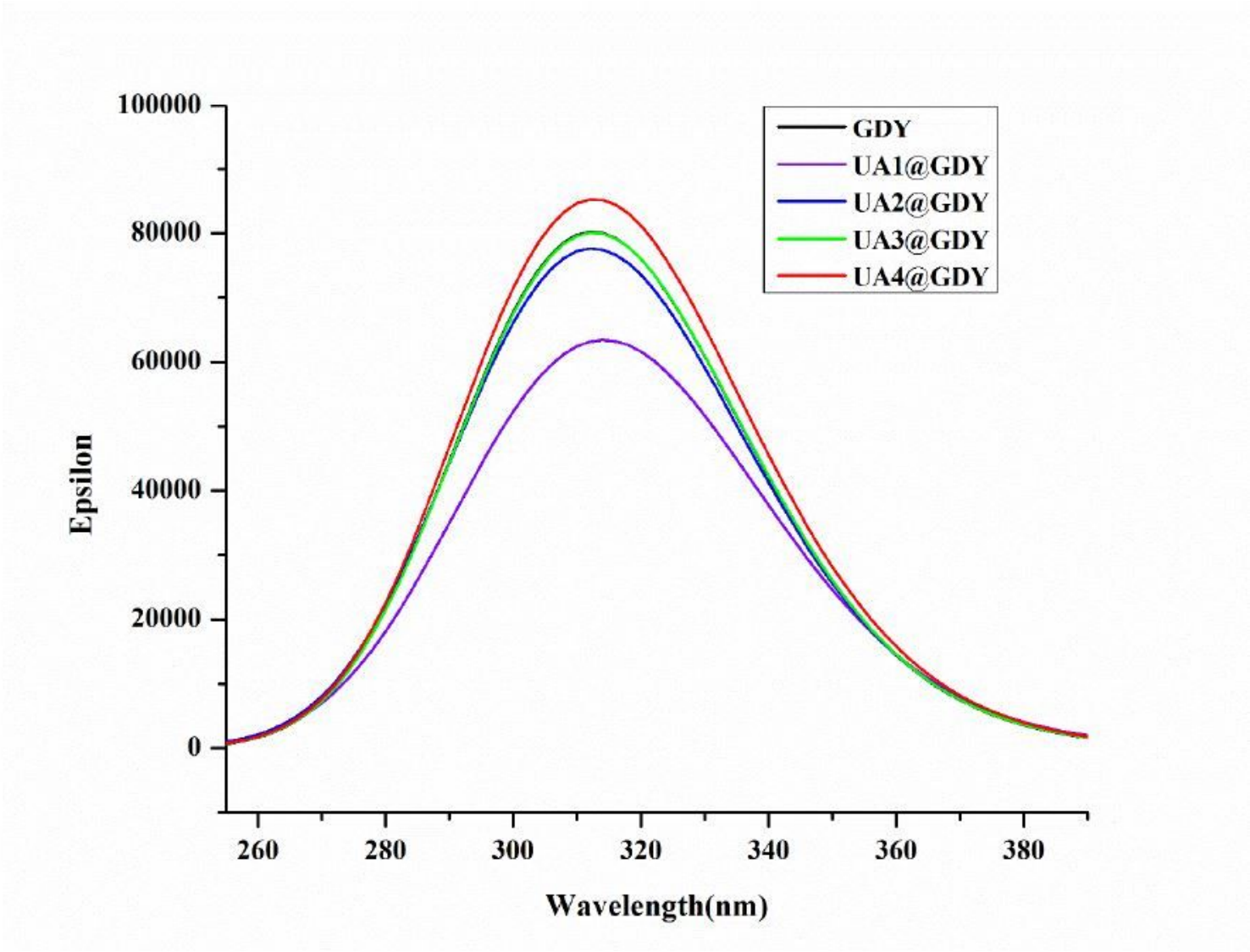

Figure 6

UV-vis spectra of UA@GDY complexes.

Supplementary Files

This is a list of supplementary files associated with this preprint. Click to download.

- Supportinginformation.docx
- GraphicalAbstract.docx